Inorganic Chemistry

Article

pubs.acs.org/IC

Lanthanide–Organic Coordination Frameworks Showing New 5-Connected Network Topology and 3D Ordered Array of Single-Molecular Magnet Behavior in the Dy Case

Min Chen,[†] E. Carolina Sañudo,[‡] Erika Jiménez,[§] Shao-Ming Fang,[†] Chun-Sen Liu,*[,†] and Miao Du*[,∥]

[†]Henan Provincial Key Lab of Surface & Interface Science, Zhengzhou University of Light Industry, Zhengzhou 450002, Henan People's Republic of China

[‡]Institut de Nanociència i Nanotecnologia i Departament de Química Inorgànica, Universitat de Barcelona, Diagonal, 647, 08028-Barcelona, Spain

[§]European Synchrotron Radiation Facility, Beamline ID-08, ESRF, 38000 Grenoble, France

[∥]College of Chemistry, Tianjin Key Laboratory of Structure and Performance for Functional Molecules, MOE Key Laboratory of Inorganic–Organic Hybrid Functional Material Chemistry, Tianjin Normal University, Tianjin 300387, People's Republic of China

Supporting Information

ABSTRACT: Five isostructural lanthanide–organic coordination frameworks with a unique 3-D 5-connected $(4^7.6^3)(4^3.6^5.8^2)$ network, namely, $[Ln(phen)(L)]_n$ (Ln = Dy for **1**, Gd for **2**, Ho for **3**, Er for **4**, and Tb for **5**), have been prepared based on bridging 5-hydroxyisophthalic acid (H_3L) and chelating 1,10-phenanthroline (phen) coligand. Significantly, the Dy(III) complex **1** is an organized array of single-molecular magnets (SMMs), with frequency-dependent out-of-phase ac susceptibility signals and magnetization hysteresis at 4 K. Further analysis of the magnetic results can reveal that the SMM behavior of **1** should arise from the smaller ferromagnetic interaction between the Dy(III) ions. Complex **1** was also characterized by X-ray absorption spectra, which give the clear X-ray magnetic circular dichroism signal.

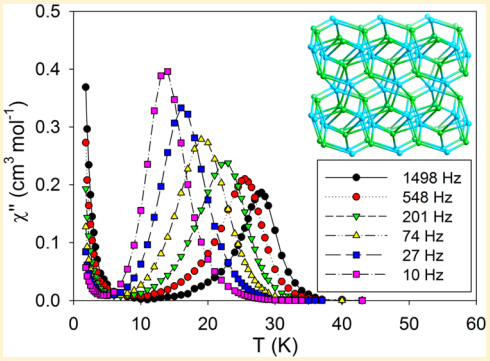

INTRODUCTION

The realm of crystal engineering has been flourishing,[1] and the crystal engineering technique has been widely used for the rational design and controlled synthesis of diverse lanthanide–organic frameworks (LnOFs) owing to their fascinating structural topologies.[2] Normally, lanthanide ions tend to coordinate with the O-donor ligands in higher and flexible coordination numbers (CNs), compared with the d-block transition-metal (TM) ions. In this regard, carboxylic acids can generally cater for the oxophilic nature of Ln ions and also, their ability to take different binding fashions fits well with the irregular coordination geometries of 4f metals.[3] Several synthetic strategies have been developed to prepare such crystalline materials with desired structures and properties, among which the appropriate choice of predesigned organic bridging ligands and lanthanide ions or clusters is one of the most effective ways.[1,4]

Molecular magnets attract much attention for their potential applications in information storage, molecular electronics, MRI imaging, among other possible applications.[5] In molecular magnetism, the research on single-molecular magnets (SMMs) is one of the most hottest areas since the 1990s.[6,7] Slow relaxation of magnetization is the intrinsic characteristic of SMMs, resulting in each single molecule behaving as a magnet. This magnet-like behavior below a blocking temperature arises from the combination of an appreciable spin ground state (S) and a negative uniaxial magnetic anisotropy (D),[8] producing the energy barrier U given by the expressions $U = S^2|D|$ for integer and $U = (S^2 - 1/4)|D|$ for half-integer spins. At the beginning of SMMs investigation, many SMMs based on high nuclearity first-row transition-metal clusters with high-spin ground states, such as Co_{24},[9] Mn_{12},[10] and Mn_{25},[11] have been reported. Meanwhile, the strong spin–orbit coupling in certain lanthanide ions (Dy^{III} and Tb^{III} and so on) results in strong magnetic anisotropy of their complexes and thus higher blocking temperatures, compared with those of first-row transition-metal SMMs. In fact, new synthetic strategies have been explored to achieve high blocking temperature and high energy barrier coordination structures. Consequently, the search for new 3d–4f architectures as well as pure 4f systems will be of great significance. In most reported lanthanide SMMs, the magnet-like behavior reveals single-ion relaxation mechanisms.[12] To move the molecular magnet materials toward practical application, more transparent insights of the relaxation mechanism are required.

Furthermore, the fascinating long-lived and narrow emission bands from near-infrared to visible regions of lanthanide ions

Received: March 3, 2014
Published: June 17, 2014

   dx.doi.org/10.1021/ic500490x | Inorg. Chem. 2014, 53, 6708–6714

Table 1. Crystallographic Data and Structural Refinement Summary for 1−5[a]

	1	2	3
empirical formula	$C_{20}H_{11}DyN_2O_5$	$C_{20}H_{11}GdN_2O_5$	$C_{20}H_{11}HoN_2O_5$
formula weight	521.81	516.56	524.24
crystal system	monoclinic	monoclinic	monoclinic
space group	$P2_1/n$	$P2_1/n$	$P2_1/n$
a/Å	9.7431(2)	9.7723(6)	9.7320(6)
b/Å	13.9008(3)	13.8718(8)	13.9346(8)
c/Å	12.0310(2)	12.0958(7)	11.9536(8)
β/°	97.243(2)	97.200(6)	97.326(6)
V/Å^3	1616.44(6)	1626.77(17)	1607.81(17)
Z	4	4	2
D/g cm^{-3}	2.144	2.109	2.166
μ/mm^{-1}	4.662	4.116	4.960
R_{int}	0.0301	0.0467	0.0677
GOF	1.033	1.007	1.003
T/K	294(2)	294(2)	294(2)
$R_1{}^a/wR_2{}^b$ $[I > 2\sigma(I)]$	0.0274/0.0630	0.0366/0.090	0.0406/0.0831
	4	**5**	
empirical formula	$C_{20}H_{11}ErN_2O_5$	$C_{20}H_{11}TbN_2O_5$	
formula weight	526.57	518.23	
crystal system	monoclinic	monoclinic	
space group	$P2_1/n$	$P2_1/n$	
a/Å	9.6993(7)	9.7851(11)	
b/Å	13.9504(10)	13.9179(16)	
c/Å	11.9486(8)	12.1056(14)	
β/°	97.382(6)	97.2270(10)	
V/Å^3	1603.4(2)	1635.5(3)	
Z	2	4	
D/g cm^{-3}	2.181	2.105	
μ/mm^{-1}	5.274	4.363	
R_{int}	0.0606	0.0217	
GOF	1.058	1.051	
T/K	294(2)	294(2)	
$R_1{}^a/wR_2{}^b$ $[I > 2\sigma(I)]$	0.0595/0.1476	0.0166/0.0382	

[a] $R_1 = \sum(||F_o| - |F_c||)/\sum|F_o|$. [b] $wR_2 = [\sum w(|F_o|^2 - |F_c|^2)^2/\sum w(F_o^2)^2]^{1/2}$.

make them good candidates for new multifunctional magnetic and luminescent materials. Though the rational design and construction of multifunctional materials with two or more physical properties is still an exciting challenge, the combination of molecular magnet behavior and luminescent properties in the same entity for lanthanide−organic coordination frameworks has come true in a few instances.[13] Herein, we present a series of lanthanide−organic coordination frameworks $[Ln(phen)(\mathbf{L})]_n$ (Ln = Dy for **1**, Gd for **2**, Ho for **3**, Er for **4**, and Tb for **5**, phen = 1,10-phenanthroline, and $H_3\mathbf{L}$ = 5-hydroxyisophthalic acid), in which complex **1** shows interesting SMM behavior and luminescent properties. The magnetic properties of other complexes have also been investigated for comparison.

EXPERIMENTAL SECTION

Materials and Physical Measurements. All reagents and solvents were obtained commercially and used as received. Fourier transform (FT) IR spectra (KBr pellets) were recorded in the range of 4000−400 cm^{-1} on a Tensor 27 OPUS (Bruker) FT-IR spectrometer. Elemental analyses (C, H, and N) were performed on a Vario EL III elemental analyzer. Thermogravimetric analysis (TGA) experiments were carried out on a PerkinElmer Diamond SII thermal analyzer in the temperature range of 25−900 °C at a heating rate of 10 °C/min under a nitrogen atmosphere with an empty Al_2O_3 crucible as the reference. Powder X-ray diffraction (PXRD) patterns were recorded on a Bruker D8 Advance diffractometer (Cu−Kα, λ = 1.54056 Å) at 40 kV and 30 mA, by using a Cu-target tube and a graphite monochromator. The powder samples were prepared by crushing the crystals, and the intensity data were recorded by continuous scan in a $2\theta/\theta$ mode from 5° to 80° with a step size of 0.02° and a scan speed of 2°/min. Simulation of the PXRD spectra was carried out by the single-crystal data and diffraction-crystal module of the Mercury (Hg) program. The emission/excitation spectra of the solid samples were recorded on an F-7000 (Hitachi) spectrophotometer at room temperature. Magnetic measurements were carried out in the Unitat de Mesures Magnètiques (Universitat de Barcelona) on polycrystalline samples (ca. 30 mg) with a Quantum Design SQUID MPMS-XL magnetometer equipped with a 5 T magnet. Diamagnetic corrections were calculated using Pascal's constants, and an experimental correction for the sample holder was applied.

Preparation of Complexes 1−5. A mixture of Ln_2O_3 (0.3 mmol, Ln = Dy for **1**, Gd for **2**, Ho for **3**, Er for **4**) or Tb_4O_7 (0.15 mmol, for **5**), $H_3\mathbf{L}$ (0.3 mmol), phen (0.15 mmol), and H_2O (15 mL) was sealed in a Teflon-lined autoclave (23 mL), heated in an oven at 170 °C for 5 days, and then cooled to room temperature at a rate of 5 °C h^{-1}. Single crystals of **1**−**5** suitable for X-ray diffraction were obtained.

For **1**: Yield ca. 30%. Anal. Calcd for $C_{20}H_{11}DyN_2O_5$: C, 46.03; H, 2.12; N, 5.37%. Found: C, 46.19; H, 2.27; N, 5.51%. IR (cm^{-1}): 3392 (m, br), 2974 (w), 2364 (w), 1617 (s), 1562 (s), 1428 (vs), 1375 (vs), 1315 (s), 1147 (w), 1126 (w), 1096 (w), 1049 (w), 1010 (s), 914 (w), 883 (w), 864 (w), 858 (w), 847 (w), 784 (s), 730 (s), 710 (s), 638 (w), 605 (m), 446 (w).

dx.doi.org/10.1021/ic500490x | Inorg. Chem. 2014, 53, 6708−6714

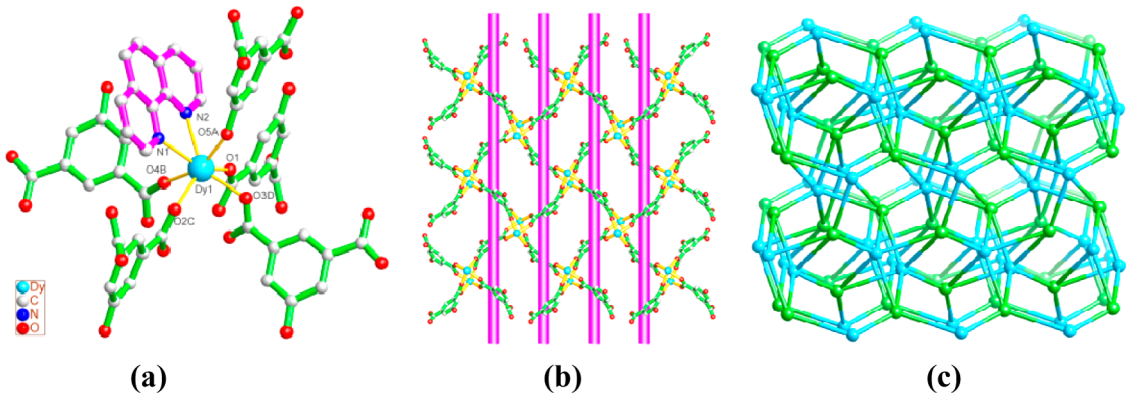

Figure 1. (a) Local coordination environment of Dy^{III} (symmetry codes for A = $-x + 1, -y + 1, -z + 1$; B = $x - 1/2, -y + 1/2, z - 1/2$; C = $-x, -y + 1, -z + 1$; D = $-x + 1/2, y + 1/2, -z + 3/2$). (b) The 2-D layer constructed by **L** ligands and Dy^{III} ions running parallel to *ac* plane. (c) Schematic representation of the 5-connected $(4^7.6^3)(4^3.6^5.8^2)$ topology.

For **2**: Yield ca. 25%. Anal. Calcd for $C_{20}H_{11}GdN_2O_5$: C, 46.50; H, 2.15; N, 5.42%. Found: C, 46.62; H, 2.29; N, 5.58%. IR (cm^{-1}): 3586 (s), 3401 (m, br), 1612 (s), 1561 (vs), 1428 (vs), 1376 (vs), 1316 (s), 1279 (w), 1147 (w), 1123 (w), 1102 (w), 1010 (m), 987 (w), 908 (w), 883 (w), 848 (m), 821 (w), 786 (s), 732 (w), 725 (w), 711 (m), 637 (w), 601 (m), 448 (m).

For **3**: Yield ca. 35%. Anal. Calcd for $C_{20}H_{11}HoN_2O_5$: C, 45.82; H, 2.11; N, 5.34%. Found: C, 45.96; H, 2.28; N, 5.49%. IR (cm^{-1}): 3429 (m, br), 1618 (s), 1562 (vs), 1428 (vs), 1376 (vs), 1317 (s), 1147 (w), 1126 (w), 1103 (w), 1010 (m), 915 (w), 883 (w), 849 (m), 784 (s), 730 (m), 710 (m), 639 (w), 605 (w), 580 (w), 447 (w).

For **4**: Yield ca. 40%. Anal. Calcd for $C_{20}H_{11}ErN_2O_5$: C, 45.62; H, 2.11; N, 5.32%. Found: C, 45.68; H, 2.17; N, 5.47%. IR (cm^{-1}): 3595 (s), 3354 (m, br), 2974 (w), 2360 (w), 1616 (s), 1560 (m), 1383 (m), 1317 (s), 1280 (s), 1147 (w), 1128 (s), 1102 (s), 1050 (w), 1008 (s), 1010 (s), 984 (s), 915 (s), 884 (w), 866 (w), 847 (w), 818 (s), 803 (s), 784 (vs), 726 (vs), 710 (s), 635 (w), 603 (w), 557 (w), 521 (w), 457 (w).

For **5**: Yield: ca. 30%. Anal. Calcd for $C_{20}H_{11}TbN_2O_5$: C, 46.35; H, 2.14; N, 5.41%. Found: C, 46.51; H, 2.21; N, 5.53%. IR (cm^{-1}): 3736 (w), 3371 (m, br), 2974 (s), 2841 (w), 1923 (w), 1616 (s), 1562 (vs), 1428 (vs), 1376 (vs), 1316 (s), 1123 (w), 1091 (s), 1050 (s), 1010 (m), 910 (w), 883 (w), 846 (m), 784 (s), 708 (m), 636 (w), 603 (w), 447 (w).

X-ray Crystallography. Single-crystal X-ray diffraction data for complexes **1**−**5** were collected on a Bruker Apex II CCD diffractometer at 294(2) K with Mo Kα radiation (λ = 0.71073 Å). A semiempirical absorption correction was applied using SADABS, and the program SAINT was used for integration of the diffraction profiles.[14] The structures were solved by direct methods with the SHELXS program of the SHELXTL package and refined with SHELXL.[15] The non-H atoms were modeled with anisotropic thermal parameters and refined by full-matrix least-square methods on F^2. In general, C-bound hydrogen atoms were placed geometrically and refined as riding. Further details for crystallographic data and refinement conditions are listed in Table 1. Selected bond parameters are shown in Tables S1−S5 (Supporting Information), respectively. CCDC-963516 (**1**), 963515 (**2**), 963518 (**3**), 963517 (**4**), and 963519 (**5**) contain the supplementary crystallographic data for this paper.

RESULTS AND DISCUSSION

Synthesis and Crystal Structures. MOFs **1**−**5** were prepared from Ln_2O_3 (for **1**−**4**) and Tb_4O_7 (for **5**) and the poly(carboxylic acid) organic ligand 5-hydroxyisophthalic acid (H_3**L**) in the presence of phen under hydrothermal conditions, which were characterized by IR spectra and microanalyses. The phase purity of bulk samples was further confirmed by PXRD patterns (Figure S1 in Supporting Information). Complexes **1**−**5** exhibit similarly high thermal stability (see Figure S2 in Supporting Information), which are thermally stable up to ca. 500 °C. Upon further heating, pyrolysis of the organic ligands occurs, which does not stop until the heating ends at 900 °C. Single-crystal X-ray structural analysis reveals that complexes **1**−**5** are isostructural (see Table 1, Tables S1−S5, and Figure S3 in Supporting Information). Thus, only the crystal structure of **1** will be discussed in detail herein. The asymmetric unit of $[Dy(phen)(\mathbf{L})]_n$ (**1**) contains one crystallographically independent Dy^{III} atom, one **L** ligand, and one phen ligand. As depicted in Figure 1a, each Dy^{III} center is seven-coordinated with a distorted pentagonal-bipyramidal geometry, which is defined by two N-donor atoms of one phen ligand [Dy−N = 2.544(4) and 2.573(4) Å], four carboxylate oxygen atoms of four **L** ligands [$Dy-O_{carboxylate}$ = 2.291(3)−2.369(3) Å], and one hydroxyl oxygen atom of **L** ligand [$Dy-O_{hydroxyl}$ = 2.168(3) Å]. The **L** ligand adopts a fully deprotonated μ_5-bridging fashion to connect five Dy^{III} centers, through the *syn*−*syn* and *syn*−*anti* binding carboxylate groups, as well as the monodentate hydroxyl oxygen atom. Such a fully deprotonated form for the aromatic hydroxyl/carboxyl ligands have also been observed in quite a few Ln coordination polymers.[2f−h] Two adjacent Dy^{III} atoms are bridged by four carboxylate groups to form a paddle-wheel motif with a Dy···Dy distance of 4.097(2) Å. Each ligand links two such paddle-wheel motifs by the carboxylate groups to result in a left- or right-handed helical chain parallel to the *b* axis with the pitch of 13.92 Å. The chains with opposite chirality are alternately arranged to afford a 2-D corrugated layer by sharing the paddle-wheel motifs (see Figure 1b). The adjacent layers are further extended by Dy−O5 interactions to construct the final 3-D network (see Figure S4 in Supporting Information).

To fully understand the complicated network structure of **1**, the topological approach is applied to simplify this 3-D coordination framework. In this approach, when the ligands and Dy^{III} centers are considered as the network nodes, such two kinds of 5-connected nodes are connected to form a 3-D 5-connected network (Figure 1c) with the point symbol of $(4^7.6^3)(4^3.6^5.8^2)$. Significantly, the 5-connected nodes usually result in a $(4^4.6^6)$ or $(4^6.6^4)$ topological network, and such a case observed in **1** represents a new structural paradigm. Alternatively, each ligand can also be viewed as a 3-connected node and each paddle-wheel dinuclear Dy^{III} unit as a 6-connected node, respectively. Thus, the overall framework can also be described as a (3,6)-connected **rtl** topology (see Figure

dx.doi.org/10.1021/ic500490x | *Inorg. Chem.* 2014, 53, 6708−6714

S5 in Supporting Information) with the point symbol of $(4.6^2)(4^2.6^{10}.8^3)$.[16]

Magnetic Studies. Magnetic susceptibility data for $[Ln(phen)(\mathbf{L})]_n$ (Ln = Dy for **1**, Gd for **2**, Ho for **3**, Er for **4**, and Tb for **5**) were collected at an applied field of 0.3 T in the 2−300 K temperature range and at an additional field on 200 Oe in 30−2 K. The data are shown in Figure 2 as χT vs T plots.

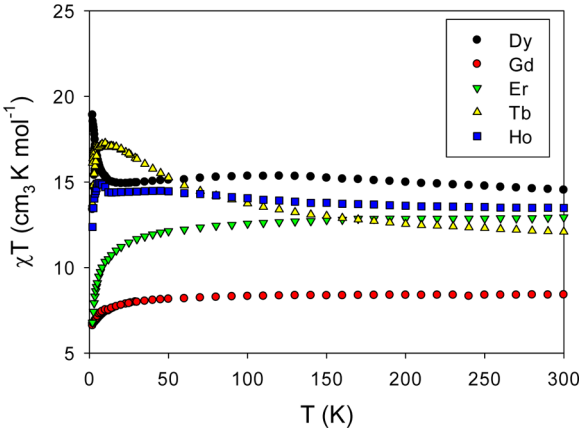

Figure 2. χT vs T plots for $[Ln(phen)(\mathbf{L})]_n$ (Ln = Dy for **1**, Gd for **2**, Ho for **3**, Er for **4**, and Tb for **5**) at 0.3 T applied field.

The χT products of the different complexes at 300 K have values of Dy (**1**) = 14.5 cm^3 K mol^{-1}, Gd (**2**) = 8.4 cm^3 K mol^{-1}, Ho (**3**) = 13.4 cm^3 K mol^{-1}, Er (**4**) = 12.9 cm^3 K mol^{-1}, and Tb (**5**) = 12.8 cm^3 K mol^{-1}, which agree well with the expected values for one free Ln^{III} ion with spin−orbit coupling: Dy^{III} = 14.16 cm^3 K mol^{-1} ($^6H_{15/2}$, $S = 5/2$, $L = 5$, $J = 15/2$, and $g_J = 4/3$),[17] Gd^{III} = 7.9 cm^3 K mol^{-1} ($^8S_{7/2}$, $S = 7/2$, $L = 0$, $g = 2.0$), Ho^{III} = 14 cm^3 K mol^{-1} ($^5I_8$, $S = 2$, $L = 6$, $J = 8$, and $g_J = 5/4$), Er^{III} = 11.81 cm^3 K mol^{-1} ($^4I_{15/2}$, $S = 3/2$, $L = 6$, $J = 15/2$, and $g_J = 6/5$), and Tb^{III} = 11.81 cm^3 K mol^{-1} ($^7F_6$, $S = 3$, $L = 3$, $J = 6$, and $g_J = 3/2$). As can be clearly observed from the χT vs T plot for the Er complex **4**, as the temperature decreases, the depopulation of the excited Stark sublevels leads to a decrease in the χT product, whereas, for the Gd complex **2**, the χT vs T plot is nearly constant, only decreasing at temperatures below 25 K, indicating practically uncoupled ions or a weak antiferromagnetic coupling. For the lanthanide complexes of Tb (**5**), Dy (**1**), and Ho (**3**), the χT vs T plots indicate the onset of weak ferromagnetic magnetic coupling below 50 K. This is confirmed by the Curie−Weiss plots shown in Figure S6 (Supporting Information) and the fitting results of the susceptibility to the Curie−Weiss law, which are summarized in Table S6 (Supporting Information). For complexes Gd (**2**) to Er (**4**), as the number of f electrons grows, the Weiss constant θ goes from small and negative (indicating antiferromagnetic interactions) to positive, and then small and negative again for Er (**4**). However, Tb (**5**), Dy (**1**) and Ho (**3**) show positive Weiss constant values, which indicate the prevalence of ferromagnetic coupling. This is unusual for Ho^{III} dimers, but not unprecedented. For example, Tong et al. have reported a Ho^{III} dimer with ferromagnetic coupling similar to that found in **3**.[21] The coordination geometries of the lanthanide ions in both cases are similar: Tong's complex is between a capped octahedron and a distorted capped trigonal prism, whereas the complex reported herein is closer to the capped trigonal prism (see Figure S8 and Table S7 in the Supporting Information). As usual for the Ln^{III} ions, this coupling is always weak, as reflected by the θ values (see Table S6 in Supporting Information), always below |10| K. This is to be expected from the detailed analysis of crystal structures (Figure 1 and Figures S3−S5, Supporting Information). The shortest Ln···Ln distances within the paddle-wheel dimers are ca. 4 Å in complexes **1**−**5**, with no monatomic bridge to enforce a good pathway for the magnetic exchange. The shortest interdimer Ln···Ln distances are ca. 7.53 Å for **1**, 7.58 Å for **2**, 7.51 Å for **3**, 7.48 Å for **4**, and 7.58 Å for **5**, respectively. Furthermore, the donor oxygen groups of the **L** ligand are situated in *meta* with respect to each other in the central aromatic ring, favoring weak ferromagnetic coupling between the metal ions.[18]

We then proceeded to study the ac magnetic susceptibility of this series of complexes, in order to clarify if the magnetic coupling can lead to long-range magnetic ordering or SMM-type behavior in these 3-D systems. The results reveal that only the Dy^{III} complex **1** shows a decrease of the in-phase signal accompanied by the appearance of an out-of-phase signal between 40 and 5 K that is frequency-dependent (see Figure 3). Below 5 K, a tail of another out-of-phase signal is observed,

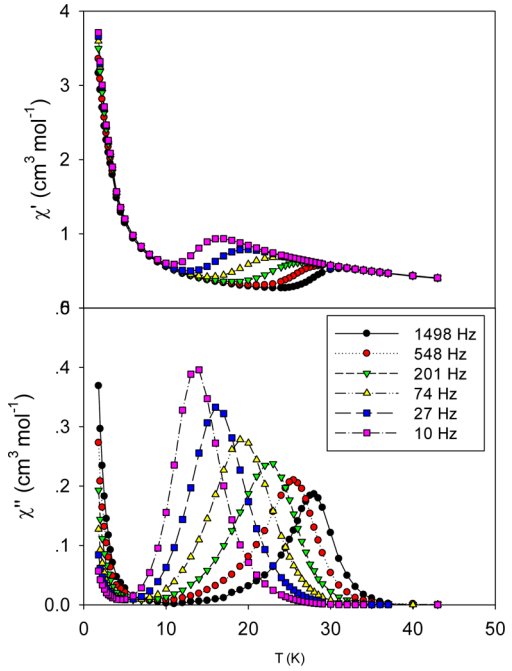

Figure 3. ac magnetic susceptibility with a 4 Oe oscillating field at various frequencies and no applied dc field for $[Dy(phen)(\mathbf{L})]_n$ (**1**). The lines are only a guide for the eye.

indicating a faster relaxation process. Analysis of the relaxation dynamics by using the Arrhenius equation shows that the process centered at 20 K has a $\tau_o = 1.6 \times 10^{-6}$ s and an effective barrier of ΔE = 131 K (see Figure 4), with a Mydosh parameter of 0.29, in agreement with the expected values for an SMM. The relaxation dynamics were also studied by measuring ac susceptibility as a function of frequency. The Cole−Cole plot (see Figure S7, Supporting Information) reveals a distribution of energy barriers with an α value of 0.03, indicating more than one possible relaxation pathway for **1**.

The value of the pre-exponential parameter indicates that the relaxation process observed in **1** is not due to long-range order and is similar to those reported for mononuclear SMMs or single-ion magnets (SIMs) of Dy^{III}.[19] Magnetization hysteresis

dx.doi.org/10.1021/ic500490x | Inorg. Chem. 2014, 53, 6708−6714

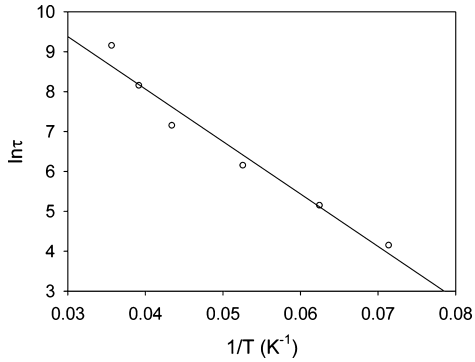

Figure 4. Arrhenius plot for the ac out-of-phase signal of complex **1** between 5 and 40 K. See text for fitting parameters.

vs field data were collected at 2 and 4 K on a Teflon-coated pressed pellet of crushed crystalline complex **1**. There is a clear hysteresis loop of the magnetization vs field at 2 and 4 K for **1** (see Figure 5). It is known that the *M*−*H* loops of transition-

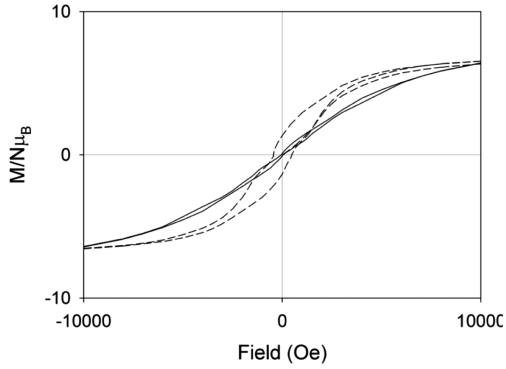

Figure 5. Magnetization vs field hysteresis loops for **1** at 2 K (dashed line) and 4 K (solid line).

metal-cluster SMMs show steps in the hysteresis due to faster relaxation via resonant tunneling of the magnetization (QTM), but sometimes these are not so clear for lanthanide-based SMMs.

In transition-metal (TM) complexes, the QTM process will happen when the applied magnetic field is sufficient to reach a level crossing between *S* substates due to the Zeeman effect. However, for the lanthanide complexes, the level crossing does not usually occur at the magnetic fields used in the experiment due to the large energy difference between the lowest and the second lowest M_J substates. Below 5 K, the out-of-phase magnetic susceptibility shows the tail of a signal that could be caused by the fast quantum tunneling typical of lanthanide complexes, and the frequency dependence of which cannot be assessed since the maxima are not observed above 2 K. Application of a dc field of up to 1500 Oe shifts this signal to lower temperatures but does not make it disappear. The Dy^{III} example **1** is the only complex to display an out-of-phase signal in the ac magnetic susceptibility in this work, thus the only one to be able to retain the magnetization when an applied field is removed below a blocking temperature and to behave as a physically ordered array of SMMs. Complex **1** displays hysteresis of the magnetization up to 4 K. Similarly to what has been reported by Clérac et al. for the 2D arrays of transition-metal SMMs and 3d−4f SMMs,[20] a small ferromagnetic interaction seems to enhance the SMM property of **1**. When this interaction is stronger as is the case of the Tb analogue **5**, no slow relaxation is observed in the ac magnetic susceptibility and the SMM property is obliterated.

The Dy(III) complex **1** was also characterized by X-ray absorption spectra (XAS), measured at ID08 beamline of the European Synchrotron Radiation Facility (ESRF). The measurements have been performed at 7 K under 4 T applied magnetic field, and the field is applied along the beam direction. The magnetic signal has been extracted from the measurements in total electron yield mode, and no sample damaging due to radiation has been observed. Using circular polarized light and the possibility to change from positive to negative polarization allows extracting the dichroic signal (XMCD). A series of eight spectra, changing the polarization, positive (σ^+) and negative (σ^-), and the applied field ($\mathbf{M}^+$ and $\mathbf{M}^-$) to avoid experimental errors, provide an XMCD signal (see Figure 6). Magnetization

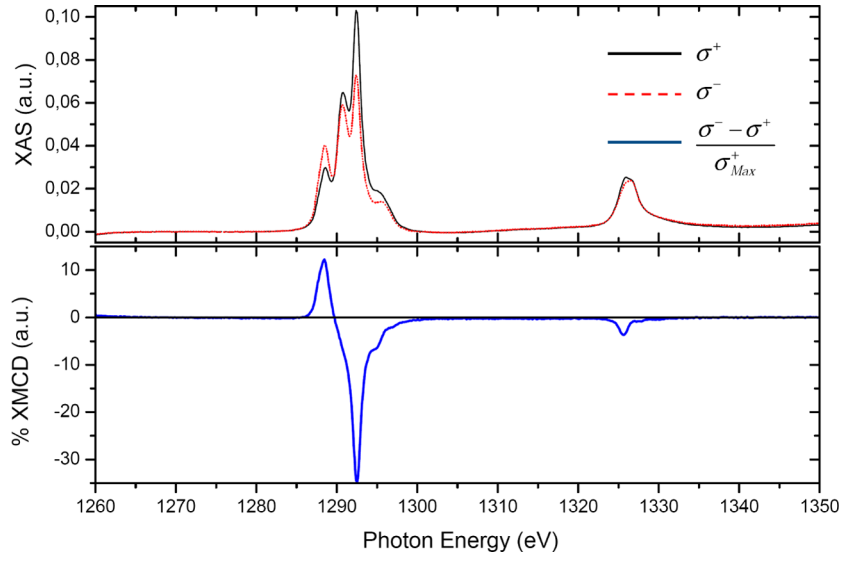

Figure 6. XAS polarization dependent spectra measured at Dy $M_{3,4}$-edges. The XMCD signal is obtained from the subtraction of the positive (σ^+) and negative (σ^-) polarized XAS, as continuous (black) and dashed (red) lines, respectively.

dx.doi.org/10.1021/ic500490x | Inorg. Chem. 2014, 53, 6708−6714

curves have been measured at the maximum of the dichroic spectra. At 7 K, the extracted hysteresis shows paramagnetic behavior.

Photoluminescence Properties. The solid-state photoluminescent spectrum for **1** shows the characteristic emission peaks at 485 and 577 nm upon excitation of the microcrystalline sample at 360 nm, which can be ascribed to the $^4F_{9/2} \rightarrow {}^6H_{15/2}$ and $^4F_{9/2} \rightarrow {}^6H_{13/2}$ transitions of Dy^{III} (see Figure S9a in Supporting Information). For **5**, the three characteristic emissions upon excitation at 370 nm (see Figure S9b in the Supporting Information) should be properly attributed to $^5D_4 \rightarrow {}^7F_J$ (J = 3, 4, 5, and 6), $^5D_4 \rightarrow {}^7F_6$ (490 nm), $^5D_4 \rightarrow {}^7F_5$ (546 nm), $^5D_4 \rightarrow {}^7F_4$ (586 nm), and $^5D_4 \rightarrow {}^7F_3$ (622 nm) transitions of Tb^{III}.

CONCLUSIONS

In conclusion, a family of lanthanide−organic coordination frameworks have been prepared based on 5-hydroxyisophthalic acid. Notably, the Dy^{III} complex **1** is an organized array of SMMs, with frequency-dependent out-of-phase ac susceptibility signals and magnetization hysteresis at 4 K. Our present findings will further enrich the crystal engineering strategy and provide the possibility of controlling the formation of desired lanthanide−organic crystalline materials. Following this lead, more efforts on H_3**L**-based coordination frameworks with other light rare-earth ions from La^{III} to Sm^{III} across the lanthanide period are underway, for developing new functional coordination polymers with higher-connected topology and interesting properties.

ASSOCIATED CONTENT

Supporting Information

Selected bond parameters (Tables S1−S5), PXRD patterns (Figure S1), TGA curves (Figure S2), further structural figures (Figures S3−S5), Curie−Weiss plots (Figure S6), Cole−Cole plot for **1** (Figure S7), Curie−Weiss fitting parameters (Table S6), continuous shape measures for the Ln(III) centers (Figure S8 and Table S7), and solid-state fluorescent spectra for **1** and **5** (Figure S9). This material is available free of charge via the Internet at http://pubs.acs.org.

AUTHOR INFORMATION

Corresponding Authors

*E-mail: chunsenliu@zzuli.edu.cn (C.-S.L.).
*E-mail: dumiao@public.tpt.tj.cn (M.D.).

Notes

The authors declare no competing financial interest.

ACKNOWLEDGMENTS

This work was supported by the National Natural Science Foundation of China (21031002, 91122005, and 21171151), Plan for Scientific Innovation Talent of Henan Province, and the Program for New Century Excellent Talents in University (NCET-10-0143). E.C.S. acknowledges the financial support from the Spanish Government (Grant CTQ2012-32247 and Ramón y Cajal contract).

REFERENCES

(1) (a) Seddon, K. R.; Zaworotko, M. *Crystal Engineering: The Design and Application of Functional Solids*; Kluwer Academic Publishers; Dordrecht, The Netherlands, 1999. (b) Desiraju, G. R. *Nature* **2001**, *412*, 397−400. (c) Janiak, C. *Dalton Trans.* **2003**, 2781−2804. (d) Robin, A. Y.; Fromm, K. M. *Coord. Chem. Rev.* **2006**, *250*, 2127−2157. (e) Robson, R. *Dalton Trans.* **2008**, 5113−5131.

(2) (a) Batten, S. R.; Neville, S. M.; Turner, D. R. *Coordination Polymers: Design, Analysis and Application*; Royal Society of Chemistry (RSC) Publishing: Cambridge, UK, 2009. (b) Furukawa, H.; Cordova, K. E.; O'Keeffe, M.; Yaghi, O. M. *Science* **2013**, *341*, 974. (c) Duan, J.-G.; Higuchi, M.; Krishna, R.; Kiyonaga, T.; Tsutsumi, Y.; Sato, Y.; Kubota, Y.; Takata, M.; Kitagawa, S. *Chem. Sci.* **2014**, *5*, 660−666. (d) Zhang, Y.-H.; Li, X.; Song, S. *Chem. Commun.* **2013**, *49*, 10397−10399. (e) Zou, R.-Q.; Sakurai, H.; Xu, Q. *Angew. Chem., Int. Ed.* **2006**, *45*, 2542−2546. (f) Gao, H.-L.; Zhao, L.; Yi, B.; Zhao, X.-Q.; Cheng, P.; Liao, D.-Z.; Yan, S.-P. *Inorg. Chem.* **2006**, *45*, 5980−5988. (g) Zhao, X.-Q.; Zhao, B.; Wei, S.; Cheng, P. *Inorg. Chem.* **2009**, *48*, 11048−11057. (h) Zhao, X.-Q.; Zhao, B.; Shi, W.; Cheng, P.; Liao, D.-Z.; Yan, S.-P. *Dalton Trans.* **2009**, 2281.

(3) (a) Champness, N. R. *Making Coordination Frameworks*; Wiley-VCH Verlag GmbH & Co. KGaA: Weinheim, Germany, 2007. (b) MacGillivray, L. R. *Metal-Organic Frameworks: Design and Application*; John Wiley & Sons, Inc.: Hoboken, NJ, 2010. (c) Schröder, M. *Functional Metal-Organic Frameworks: Gas Storage, Separation and Catalysis*; Springer: Berlin, Germany, 2010.

(4) Du, M.; Li, C.-P.; Liu, C.-S.; Fang, S.-M. *Coord. Chem. Rev.* **2013**, *257*, 1282−1305.

(5) (a) Leuenberger, M. N.; Loss, D. *Nature* **2001**, *410*, 789−793. (b) Gatteschi, D.; Sessoli, R. *Angew. Chem., Int. Ed.* **2003**, *42*, 268−297. (c) Bogani, L.; Wernsdorfer, W. *Nat. Mater.* **2008**, *7*, 179−186. (d) Vincent, R.; Klyatskaya, S.; Ruben, M.; Wernsdorfer, W.; Balestro, F. *Nature* **2012**, *488*, 357−360.

(6) (a) Mannini, M.; Pineider, F.; Danieli, C.; Totti, F.; Sorace, L.; Sainctavit, Ph.; Arrio, M.-A.; Otero, E.; Joly, L.; Cezar, J. C.; Cornia, A.; Sessoli, R. *Nature* **2010**, *468*, 417−421. (b) Long, J.; Habib, F.; Lin, P.-H.; Korobkov, I.; Enright, G.; Ungur, L.; Wernsdorfer, W.; Chibotaru, L. F.; Murugesu, M. *J. Am. Chem. Soc.* **2011**, *133*, 5319−5328. (c) Cardona-Serra, S.; Clemente-Juan, J. M.; Coronado, E.; Gaita-Ariño, A.; Camón, A.; Evangelisti, M.; Luis, F.; Martínez-Pérez, M. J.; Sesé, J. *J. Am. Chem. Soc.* **2012**, *134*, 14982−14990. (d) Zhu, Y.-Y.; Cui, C.; Zhang, Y.-Q.; Jia, J.-H.; Guo, X.; Gao, C.; Qian, K.; Jiang, S.-D.; Wang, B.-W.; Wang, Z.-M.; Gao, S. *Chem. Sci.* **2013**, *4*, 1802−1806.

(7) (a) Hewitt, I. J.; Tang, J.; Madhu, N. T.; Anson, C. E.; Lan, Y.; Luzon, J.; Etienne, M.; Sessoli, R.; Powell, A. K. *Angew. Chem., Int. Ed.* **2010**, *49*, 6352−6356. (b) Rinehart, J. D.; Fang, M.; Evans, W. J.; Long, J. R. *Nat. Chem.* **2011**, *3*, 538−542. (c) Gatteschi, D.; Sessoli, R. *Angew. Chem., Int. Ed.* **2003**, *42*, 268−297. (d) Liu, J.-L.; Chen, Y.-C.; Li, Q.-W.; Gómez-Coca, S.; Aravena, D.; Ruiz, E.; Lin, W.-Q.; Leng, J.-D.; Tong, M.-L. *Chem. Commun.* **2013**, *49*, 6549−6551.

(8) Christou, G.; Gatteschi, D.; Hendrickson, D. N.; Sessoli, R. *MRS Bull.* **2000**, *25*, 66−77.

(9) (a) Liu, C.-M.; Zhang, D.-Q.; Hao, X.; Zhu, D.-B. *Chem. - Eur. J.* **2011**, *17*, 12285−12288. (b) Han, S.-D.; Song, W.-C.; Zhao, J.-P.; Yang, Q.; Liu, S.-J.; Lia, Y.; Bu, X.-H. *Chem. Commun.* **2013**, *49*, 871−873.

(10) (a) Sessoli, R.; Tsai, H.-L.; Schake, A. R.; Wang, S.; Vincent, J. B.; Folting, K.; Gatteschi, D.; Christou, G.; Hendrickson, D. N. *J. Am. Chem. Soc.* **1993**, *115*, 1804−1816. (b) Lampropoulos, C.; Murugesu, M.; Harter, A. G.; Wernsdofer, W.; Hill, S.; Dalal, N. S.; Reyes, A. P.; Kuhns, P. L.; Abboud, K. A.; Christou, G. *Inorg. Chem.* **2013**, *52*, 258−272. (c) Wang, H.; Hamanaka, S.; Yokoyama, T.; Yoshikawa, H.; Awaga, K. *Chem. - Asian J.* **2011**, *6*, 1074−1079.

(11) (a) Stamatatos, T. C.; Abboud, K. A.; Wernsdorfer, W.; Christou, G. *Angew. Chem., Int. Ed.* **2007**, *46*, 884−888. (b) Murugesu, M.; Habrych, M.; Wernsdorfer, W.; Abboud, K. A.; Christou, G. *J. Am. Chem. Soc.* **2004**, *126*, 4766−4767. (c) Murugesu, M.; Takahashi, S.; Wilson, A.; Abboud, K. A.; Wernsdorfer, W.; Hill, S.; Christou, G. *Inorg. Chem.* **2008**, *47*, 9459−9470.

(12) (a) Lin, P.-H.; Burchell, T. J.; Ungur, L.; Chibotaru, L. F.; Wernsdorfer, W.; Murugesu, M. *Angew. Chem., Int. Ed.* **2009**, *48*, 9489−9492. (b) Blagg, R. J.; Muryn, C. A.; McInnes, E. J. L.; Tuna, F.; Winpenny, R. E. P. *Angew. Chem., Int. Ed.* **2011**, *50*, 6530−6533.

(c) Jiang, S.-D.; Wang, B.-W.; Sun, H.-L.; Wang, Z.-M.; Gao, S. *J. Am. Chem. Soc.* **2011**, *133*, 4730−4733.
(13) (a) Dei, A. *Angew. Chem., Int. Ed.* **2005**, *44*, 1160−1163. (b) Sato, O.; Tao, J.; Zhang, Y.-Z. *Angew. Chem., Int. Ed.* **2007**, *46*, 2152−2187. (c) Sato, O.; Iyoda, T.; Fujishima, A.; Hashimoto, K. *Science* **1996**, *272*, 704−705. (d) Li, D.; Clérac, R.; Roubeau, O.; Harté, E.; Mathonière, C.; Bris, R. L.; Holmes, S. M. *J. Am. Chem. Soc.* **2008**, *130*, 252−258. (e) Liu, C.-S.; Du, M.; Sañudo, E. C.; Echeverria, J.; Zhang, Q.; Zhou, L.-M.; Fang, S.-M. *Dalton Trans.* **2011**, *40*, 9366−9369.
(14) *SAINT Software Reference Manual*; Bruker AXS: Madison, WI, 1998.
(15) Sheldrick, G. M. *SHELXTL NT: Program for Solution and Refinement of Crystal Structures*, Version 5.1; University of Göttingen: Göttingen, Germany, 1997.
(16) Blatov, V. A.; Shevchenko, A. P. *TOPOS-Version 4.0 professional (beta evaluation)*; Samara State University: Samara, Russia, 2006.
(17) Benelli, C.; Gatteschi, D. *Chem. Rev.* **2002**, *102*, 2369−2388.
(18) (a) Wang, J.; Bei, F.-L.; Yang, X.-J.; Lu, L.-D.; Wang, X. *J. Mol. Struct.* **2002**, *643*, 129−133. (b) Laye, R. H.; Sañudo, E. C. *Inorg. Chim. Acta* **2009**, *362*, 2205−2212. (c) Paital, A. R.; Mitra, T.; Ray, D.; Wong, W. T.; Ribas-Ariño, J.; Novoa, J. J.; Ribas, J.; Aromi, G. *Chem. Commun.* **2005**, 5172−5174.
(19) (a) Ishikawa, N.; Sugita, M.; Wernsdorfer, W. *Angew. Chem., Int. Ed.* **2005**, *44*, 2931−2935. (b) Ishikawa, N.; Sugita, M.; Wernsdorfer, W. *J. Am. Chem. Soc.* **2005**, *127*, 3650−3651. (c) Ishikawa, N.; Sugita, M.; Ishikawa, T.; Koshihara, S.; Kaizu, Y. *J. Phys. Chem. B* **2004**, *108*, 11265−11271. (d) Ishikawa, N.; Sugita, M.; Okubo, T.; Tanaka, N.; Iino, T.; Kaizu, Y. *Inorg. Chem.* **2003**, *42*, 2440−2446. (e) Ishikawa, N.; Iino, T.; Kaizu, Y. *J. Am. Chem. Soc.* **2002**, *124*, 11440−11447. (f) Ishikawa, N.; Iino, T.; Kaizu, Y. *J. Phys. Chem. A* **2003**, *107*, 7879−7884. (g) Ishikawa, N.; Sugita, M.; Ishikawa, T.; Koshihara, S.; Kaizu, Y. *J. Am. Chem. Soc.* **2003**, *125*, 8694−8695.
(20) (a) Jeon, I.-R.; Ababei, R.; Lecren, L.; Li, Y.-G.; Wernsdorfer, W.; Roubeau, O.; Mathonière, C.; Clérac, R. *Dalton Trans.* **2010**, *39*, 4744−4746. (b) Jeon, I.-R.; Clérac, R. *Dalton Trans.* **2012**, *41*, 9569−9586.
(21) Leng, J.-D.; Liu, J.-L.; Lin, W.-Q.; Gómez-Coca, S.; Aravena, D.; Ruiz, E.; Tong, M.-L. *Chem. Commun.* **2013**, *49*, 9341−9343.